

Abstract

Long distance optical communication systems experience a large degree of attenuation due to fibre losses, necessitating signal amplification. Erbium Doped Fibre Amplifiers (EDFAs) have found widespread use as all-fibre optical amplifiers, but exhibit unequal amplification of different wavelengths. Since the gain spectrum is signal-power and pump-power dependent, each EDFA spectrum may differ considerably, and a tuneable gain equalizer is required. A tuneable long-period grating (LPG) can be implemented as a gain equalizer for EDFAs.

This dissertation deals with the design of an integrated optic version of the tuneable equalizing filter. The various components of which the device comprises, including optical couplers, Mach-Zehnder interferometers and an LPG, are investigated. The integrated optics designs of these components are then done using the BeamPROP software package. The use and optical properties of germania-doped silica as photosensitive waveguide material is studied. The production of the films for the gain equalizer, using electron-cyclotron resonance plasma-enhanced chemical vapour deposition, is discussed. Characterization of these films was carried out using spectroscopic ellipsometry and infrared spectroscopy. The optical constants, thickness, germania content and hydroxyl absorption was calculated using these measurements.

Contents

| | |
|---|-----------|
| 1 Introduction | 7 |
| 1.1 Background | 8 |
| 1.2 Objectives of the investigation | 9 |
| 1.3 Layout of the investigation | 9 |
| 2 Erbium Doped Fibre Amplifiers | 13 |
| 2.1 Principle of operation | 14 |
| 2.1.1 Energy levels and lifetimes | 14 |
| 2.1.2 EDFA configurations and pump wavelengths | 15 |
| 2.1.3 Influence of Er^{3+} -ion concentration | 17 |
| 2.1.4 Advantages | 18 |
| 2.2 Modelling EDFAs | 18 |
| 2.3 Gain equalizing schemes for EDFAs | 20 |
| 2.4 The tuneable LPG gain equalizer | 24 |

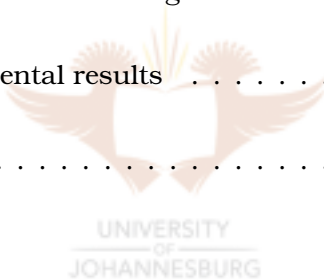
| | | |
|----------|---|-----------|
| 2.4.1 | Experimental setup of the tuneable LPG | 24 |
| 2.4.2 | Theoretical transfer function of the tuneable LPG | 24 |
| 2.4.3 | Experimental implementation of the tuneable LPG | 26 |
| 2.4.4 | The Mach-Zehnder interferometer | 28 |
| 2.5 | Conclusion | 29 |
| 3 | Integrated-optic tuneable gain equalizer | 35 |
| 3.1 | Optical properties of $GeO_2 : SiO_2$ | 36 |
| 3.1.1 | Propagation loss and bending radius | 39 |
| 3.2 | Long-period gratings | 40 |
| 3.2.1 | Introduction | 40 |
| 3.2.2 | Principle of operation | 42 |
| 3.2.3 | Simulation of an LPG | 43 |
| 3.3 | Optical couplers | 47 |
| 3.3.1 | Tuneable couplers | 50 |
| 3.4 | Designs using BeamPROP software | 52 |
| 3.4.1 | The beam propagation method | 52 |
| 3.4.2 | Simulation setup | 54 |
| 3.4.3 | 3-dB directional coupler design | 57 |
| 3.4.4 | Tuneable MZI coupler design | 60 |
| 3.4.5 | Long-period grating design | 62 |
| 3.5 | Conclusion | 64 |

| | |
|--|-----------|
| 4 Deposition of GeO_2-doped SiO_2 films | 69 |
| 4.1 ECR- PECVD | 70 |
| 4.1.1 Chemical Vapour Deposition | 70 |
| 4.1.2 Plasma processes | 71 |
| 4.1.2.1 Sheath formation[2] | 75 |
| 4.1.2.2 Pressure | 76 |
| 4.1.2.3 Electron Cyclotron Resonance | 77 |
| 4.1.2.4 Advantages of ECR-PECVD | 78 |
| 4.1.2.5 RF biasing of the substrate | 79 |
| 4.2 Domex MDECR-PECVD | 80 |
| 4.2.1 The gas distribution system | 80 |
| 4.2.2 The reactor chamber, microwave antennas and ECR magnets | 81 |
| 4.2.3 The pumping station | 84 |
| 4.2.3.1 The turbo molecular pump[8, 9] | 84 |
| 4.2.3.2 The rotary vane pump | 85 |
| 4.2.4 Pressure Gauges | 86 |
| 4.2.4.1 Pirani gauges | 86 |
| 4.2.4.2 Capacitance manometer | 87 |
| 4.2.4.3 Penning gauges | 89 |

| | | |
|----------|---|------------|
| 4.3 | The use of $GeO_2 : SiO_2$ waveguides | 90 |
| 4.3.1 | Photosensitivity | 90 |
| 4.3.2 | Optical waveguide fabrication and structure | 92 |
| 4.4 | Description of the fabrication process | 94 |
| 4.4.1 | Depositions done at the COCS | 95 |
| 4.4.2 | Deposition of $a - C : H$ | 95 |
| 4.4.3 | Deposition of SiO_2 | 96 |
| 4.4.4 | Deposition of $GeO_2 : SiO_2$ | 97 |
| 4.4.5 | Etching of the reactor | 98 |
| 4.5 | Conclusion | 99 |
| 5 | Ellipsometry | 103 |
| 5.1 | Fundamentals of ellipsometry | 104 |
| 5.1.1 | Electromagnetic formalism | 107 |
| 5.2 | Single wavelength ellipsometers | 109 |
| 5.3 | Spectroscopic ellipsometers | 111 |
| 5.4 | Modelling of ellipsometric data | 113 |
| 5.4.1 | Use of the DeltaPsi II software | 113 |
| 5.4.2 | Modelling of manufactured samples | 118 |
| 5.4.2.1 | Deposition of $a - C : H$ | 119 |
| 5.4.2.2 | Deposition of SiO_2 | 119 |
| 5.5 | Conclusion | 121 |



| | |
|--|------------|
| <i>CONTENTS</i> | viii |
| 6 Results | 125 |
| 6.1 Characterization of the photosensitive films | 126 |
| 6.2 GeO_2 content | 130 |
| 6.3 Transmission spectroscopy | 133 |
| 6.4 Conclusion | 138 |
| 7 Conclusion and future work | 141 |
| 7.1 Conclusion | 142 |
| 7.1.1 Simulations and design | 142 |
| 7.1.2 Experimental results | 142 |
| 7.2 Future work | 143 |



List of Figures

| | | |
|------|---|----|
| 2.1 | Erbium energy level diagram and stimulated emission . . . | 14 |
| 2.2 | Example of an EDFA | 16 |
| 2.3 | EDFA pumping schemes: (a) co-directional pumping (b) counter-directional pumping and (c) dual pumping. WSC: wavelength selective coupler. | 17 |
| 2.4 | EDFA gain spectrum | 20 |
| 2.5 | Tuneable MZI gain equalizer | 23 |
| 2.6 | Tuneable LPG gain equalizing filter | 24 |
| 2.7 | Example transmission spectrum of an LPG | 25 |
| 2.8 | Transmission spectrum of the TEF | 26 |
| 2.9 | Experimental determined relative attenuation spectra[8] | 27 |
| 2.10 | EDFA and flattened gain spectrum[8] | 27 |
| 3.1 | Illustration of the effective index method | 37 |
| 3.2 | Grating period calculation for various cladding modes | 41 |

| | |
|--|----|
| <i>LIST OF FIGURES</i> | 2 |
| 3.3 Operation of an LPG | 43 |
| 3.4 Normalized frequency V versus ηd | 46 |
| 3.5 Transmission of an LPG | 47 |
| 3.6 Symmetrical four-port coupler | 48 |
| 3.7 Power transfer with increased coupling length | 49 |
| 3.8 An array of lenses equivalent to the beam-shape transformation expressed by the BPM. | 53 |
| 3.9 Simulation of the fundamental mode in the XY-plane | 56 |
| 3.10 Three dimensional view of the fundamental mode | 56 |
| 3.11 Designed 3-dB directional coupler | 57 |
| 3.12 Simulation results for 3-dB directional coupler | 58 |
| 3.13 2×1 MMI coupler | 59 |
| 3.14 Designed tuneable MZI coupler | 60 |
| 3.15 Simulation results for tuneable MZI coupler | 61 |
| 3.16 Influence of temperature on the coupling ratio | 62 |
| 3.17 Designed long-period grating | 63 |
| 3.18 Simulation results for long-period grating | 63 |
| 4.1 Generic CVD system | 71 |
| 4.2 ECR Phenomenon[1] | 78 |

| | |
|---|-----|
| <i>LIST OF FIGURES</i> | 3 |
| 4.3 Domex MDECR-PECVD system | 80 |
| 4.4 Schematic of DomeX MDECR-PECVD reactor chamber . . . | 82 |
| 4.5 Plasma source | 82 |
| 4.6 Impedance matching unit | 83 |
| 4.7 Matrix distribution of the ECR microwave antennas | 83 |
| 4.8 Etching and deposition plasmas | 84 |
| 4.9 Rotor and stator discs of turbo molecular pump. | 85 |
| 4.10 Rotary vane pump. | 86 |
| 4.11 Pirani Gauge. | 87 |
| 4.12 Capacitance manometer | 88 |
| 4.13 Penning Gauge | 89 |
| 4.14 Fabrication process of a buried channel waveguide | 93 |
| 4.15 Schematic of INFRASIL substrate and GeO_2 -doped SiO_2 film | 94 |
| 5.1 Δ and Ψ vs angle of incidence | 105 |
| 5.2 Reflection of light on a surface | 107 |
| 5.3 Reflection of light from a film on a substrate | 108 |
| 5.4 The AutoEL-II Ellipsometer configuration | 110 |
| 5.5 The Phase Modulation Ellipsometer | 112 |

| | |
|---|-----|
| 5.6 Model of SiO_2 | 113 |
| 5.7 Simulated model and acquired data | 114 |
| 5.8 Dispersion of SiO_2 | 115 |
| 5.9 Model fitted to acquired data | 116 |
| 5.10 User defined (classical Lorentz oscillator) dispersion for SiO_2 | 116 |
| 5.11 Comparison between two films of different thickness | 117 |
| 5.12 SiO_2 layer grown by point injection | 120 |
| 5.13 SiO_2 layer grown by volume injection | 120 |
| 6.1 Change in refractive index with increased GeH_4 flow at 1550 nm | 126 |
| 6.2 Refractive index vs wavelength for different GeH_4 flow rates | 127 |
| 6.3 Calculated thickness at 1.5 cm spaced positions on the wafers | 128 |
| 6.4 Refractive index at 2 eV at 1.5 cm spaced positions on the wafers | 129 |
| 6.5 Dispersion relations using Sellmeier equations[1] | 131 |
| 6.6 Relation between theoretical refractive index and molar percentage GeO_2 | 131 |
| 6.7 Germane flow versus molar percentage GeO_2 | 132 |
| 6.8 Refractive index versus germane flux | 132 |
| 6.9 Transmission spectra of Infrasil substrate | 134 |

| | |
|--|-----|
| <i>LIST OF FIGURES</i> | 5 |
| 6.10 Transmission spectra of film T1 | 135 |
| 6.11 Transmission spectra of film T2 | 135 |
| 6.12 Transmission spectra of film T3 | 136 |
| 6.13 Hydroxyl absorption for T1, T2 and T3 | 137 |



List of Tables

| | |
|---|-----|
| 2.1 Summary of gain flattening methods[9] | 21 |
| 4.1 Surface reactions[2] | 73 |
| 4.2 SiO_2 and SiO_xN_y deposition | 95 |
| 4.3 Reactor conditions during SiO_2 deposition | 96 |
| 4.4 $Ge : SiO_2$ Depositions | 97 |
| 4.5 Deposition information for samples T1, T2 and T3 | 98 |
| 5.1 SiO_2 and SiO_xN_y refractive indices and thicknesses | 118 |
| 5.2 SiO_2 Growth rate | 119 |
| 6.1 $GeO_2 : SiO_2$ layers | 126 |
| 6.2 Deposition information for samples T1, T2 and T3 | 129 |
| 6.3 Estimated refractive indices at 1550 nm | 129 |
| 6.4 Sellmeier parameters | 130 |
| 6.5 Calculated molar percentage GeO_2 using Sellmeier equation and rule of mixtures | 133 |